

Surface Brightness Measurements for APM Galaxies

Z. Shao^{*1,2}, S. J. Maddox², J. B. Jones² and P. Coles²

¹*Shanghai Astronomical Observatory, Chinese Academy of Science, Shanghai 200030, P.R. China*

²*School of Physics & Astronomy, University of Nottingham, Nottingham NG7 2RD, UK*

Accepted 28 August 2002

ABSTRACT

This paper considers some simple surface brightness (SB) estimates for galaxies in the Automated Plate Measuring Machine (APM) catalogue in order to derive homogeneous SB data for a very large sample of faint galaxies. The isophotal magnitude and area are used to estimate the central surface brightness and total magnitude based on the assumption of an exponential SB profile. The surface brightness measurements are corrected for field effects on each UK Schmidt plate and the zero-point of each plate is adjusted to give a uniform sample of SB and total magnitude estimates over the whole survey. Results are obtained for 2.4 million galaxies with blue photographic magnitudes brighter than $b_J = 20.5$ covering 4300 deg^2 in the region of the south galactic cap. Almost all galaxies in our sample have central surface brightness in the range 20 to 24 $b_J \text{ mag arcsec}^{-2}$. The SB measurements we obtain are compared to previous SB measurements and we find an acceptable level of error of $\pm 0.2 b_J \text{ mag arcsec}^{-2}$. The distribution of SB profiles is considered for different galaxy morphologies for the bright APM galaxies. We find that early-type galaxies have more centrally concentrated profiles.

Key words: surveys - galaxies: photometry - surface brightness.

1 INTRODUCTION

Surface brightness (SB) is one of the fundamental parameters describing a galaxy. It plays an important role in many diverse aspects of extragalactic astronomy and cosmology, from identifying the whole family of galaxy populations to modelling their different distributions and motions in the Universe. These aspects are generally related to the formation and evolution of galaxies, as well as to the nature of large scale structures in the Universe.

Unfortunately, accurate measurements of the SB of galaxies rely critically on high quality observations with perfect sky conditions and adequate telescope time, so it is not easy to get high quality SB data for galaxies, especially for low surface brightness galaxies (LSBG). Large, homogeneous data samples are even more difficult to construct, and so uniform SB data for galaxies is very scarce compared to other parameters, such as position, colour, redshift and morphology. Hitherto relatively few sets of SB measurements have been available; the total number of such galaxies is only a few thousand, and the samples have either concentrated on LSBGs or been limited only to bright galaxies (e.g. de Jong & van der Kruit 1994; de Jong 1996; Jansen et al. 2000; Heraudeau & Simien 1996; Lauberts & Valentijn 1989;

Impey et al. 1996; Morshidi-Esslinger et al. 1999, hereafter MDS).

On the other hand it is not difficult to make a rough estimate of a galaxy's SB using parameters related to both the luminosity and size of a galaxy. These two kinds of basic parameters, such as magnitude and effective radius of galaxies, are common in many catalogues. One can consequently obtain a larger sample of SB data of galaxies at the expense of some accuracy for individual objects. The statistical analysis of a large number of galaxies will not sensitively depend on the accuracy of the SB measurement for each individual galaxy because reasonable errors in SB can be allowed for in the analysis.

The APM catalogue includes both the magnitude and isophotal size for each galaxy so these can be used to estimate the SB of galaxies. Based on this strategy, some work has already used SB estimates from the APM survey. Côté et al. (1999) used the mean isophotal SB of APM galaxies to select the candidates for an HI survey of LSBGs. More recently Cross et al. (2001) calculated the effective SB of galaxies in the 2dF Galaxy Redshift Survey and estimated their bivariate brightness distribution, as well as the number and luminosity density of galaxies.

In this paper, we consider a variety of SB estimates, and present a method for determining the central surface brightness, μ_0 , of galaxies in the APM Galaxy Survey. We apply a

* E-mail: zyshao@center.shao.ac.cn

field correction across each survey plate, and use a matching procedure over the whole survey area to yield a homogeneous SB sample of over 2 million galaxies with a wide magnitude range over a large volume of space. The results will be used in future papers to study the distribution of galaxies as a function of surface brightness, in particular their clustering properties. We describe the basic data in Section 2. The principles behind the method are described in Section 3, together with an introduction of the raw APM parameters that relate to the SB of galaxies. The field correction and matching process are briefly outlined in Section 4, where we also discuss the uncertainty of our SB estimates and compare to other SB measurements. In Section 5 we consider the distributions of μ_0 and the SB profiles of bright APM galaxies. Finally we summarize our results in Section 6.

2 THE APM CATALOGUE

The APM Galaxy Survey is hitherto the largest galaxy survey used for the investigation of the large-scale distribution of galaxies. It contains over 3 million galaxy positions and apparent magnitudes, compiled by scanning 269 UK Schmidt Telescope (UKST) survey plates over the southern sky with the Automatic Plate Measuring (APM) machine. A subset of 2.4 million galaxies in 185 UKST fields south of declination -20° , compiled from photographic data of a consistently high quality and representing the first stage of the APM survey, was described by Maddox et al. (1990a,b). This subset covered the south galactic cap and is defined by the boundaries of UKST plates whose centres have galactic latitude between $b = -30^\circ$ and -40° (the exact limit depending on star number densities, and therefore on longitude), as well as declination. It is this subset of 185 plates, representing an area of 4300 square degrees, that we use in this paper.

The APM identified images using a connected-pixel algorithm, selecting groups of 16 or more pixels having intensities above a fixed threshold optical density. With a mean pixel size of 0.51 arcsec (the plate scale varies slightly from plate to plate and across individual plates), this corresponds to a minimum area of 4.3 arcsec². The detection threshold t was set for each plate to be about twice the *rms* noise in the sky, leading to a mean threshold of 12 APM density units, corresponding to ~ 25 b_J mag arcsec⁻² above the sky background. The threshold varies within each plate due to vignetting and emulsion effects and also varies from plate to plate, because of the different photometric zero-points for each plate. The standard deviation in the threshold due to the variation in photometric zero points from plate to plate is 0.3 b_J mag arcsec⁻².

The images were classified as stars, galaxies, blended images and noise based on comparisons with the median stellar profile as a function of magnitude, as described in detail by Maddox et al. (1990a). In our present analysis we consider only images classified as galaxies. The total magnitude was estimated from the isophotal magnitude and area of each detected image, assuming a Gaussian light profile. This process was optimized for faint images near the magnitude limit where galaxy profiles are significantly affected by seeing. Different plates have different limiting magnitudes, and so to ensure a uniform limit, the final sample was fur-

ther constrained by the magnitude limit of the poorest plate, 20.5 b_J . Rejecting images fainter than 20.5 b_J in total magnitude produced the final APM Catalogue that we consider in this paper.

3 MEASUREMENT OF SURFACE BRIGHTNESS

3.1 APM data

The APM Catalogue includes measurements of the isophotal flux and the image area within the detection isophote for each image. These parameters are used here to estimate the SB of each galaxy assuming an exponential light profile. The APM parameters are calculated using emulsion density D , rather than incident flux f measurements. Below the emulsion saturation D_{\max} , it is fairly well approximated by a linear relationship,

$$D = \begin{cases} \alpha f + \beta & \text{for } f < (D_{\max} - \beta)/\alpha \\ D_{\max} & \text{for } f > (D_{\max} - \beta)/\alpha \end{cases} \quad (1)$$

where α and β are constants for any particular part of the plate (Maddox et al. 1990a,b, Cawson et al. 1987), and the value of D_{\max} is found to vary by 2% across the field (Maddox et al. 1990b). The incident flux f , is the sum of the sky flux f_{sky} , and the object flux f_{obj} . So, the APM measures the sky-subtracted density D_{obj} for particular pixels of objects, as

$$\begin{aligned} D_{\text{obj}} &= D - D_{\text{sky}} \\ &= \alpha f + \beta - (\alpha f_{\text{sky}} + \beta) \\ &= \alpha f_{\text{obj}} \end{aligned} \quad (2)$$

where $D_{\text{sky}} = \alpha f_{\text{sky}} + \beta$ is the local sky value which was obtained from a pre-scan and smoothing process (Maddox, 1988). Obviously, the upper limit of D_{obj} is, $D_{\text{sat}} = D_{\max} - D_{\text{sky}}$, for any particular position in a plate. The saturation density D_{sat} corresponds typically to a magnitude surface brightness $\simeq 22.3$ b_J mag arcsec⁻² above the sky, but this figure varies with the sky background level. Note that this saturation is quite severe: for a typical disk galaxy with a central SB of 21.4 b_J mag arcsec⁻², the profile is saturated inside 0.8 disk scale-lengths.

For each image, the APM measures the relative brightness by summing D_{obj} for pixels above the threshold t ($\simeq 25$ mag arcsec⁻²),

$$I_{\text{iso}} = \sum_{D_{\text{obj}} \geq t} D_{\text{obj}}. \quad (3)$$

The threshold t is constant across the field of each plate, but varies from plate to plate according to the fluctuation of the sky density for individual plates (Maddox et al. 1990a,b). When working with APM data it is convenient to define an ‘isophotal APM magnitude’, m_{iso} , of an image as

$$m_{\text{iso}} = +2.5 \log_{10} I_{\text{iso}} \quad (4)$$

This APM parameter is related to the actual isophotal magnitude, b_{iso} , which is given by

$$b_{\text{iso}} = Z - 2.5 \log_{10} I_{\text{iso}} \quad (5)$$

where Z is the magnitude zero-point of the photographic

plate. Also, the isophotal size of the image is given by

$$A_{\text{iso}} = \sum_{D_{\text{obj}} \geq t} 1 \quad (6)$$

I_{iso} , t and A_{iso} are the three main APM parameters that we use to measure the SB profile of galaxies. In former work on APM galaxy survey, Maddox et al. (1990b) used these parameters together with the assumption of Gaussian galaxy profiles to calculate a total APM magnitude m_{tot} which was then calibrated to b_J using CCD magnitudes. For faint galaxies near the magnitude limit of the APM survey this is a reasonable approximation, because the galaxy images are small and the profile shape is dominated by the seeing disc. But for brighter galaxies an exponential profile is a better approximation (see Section 5). In the following subsections, we mainly use these three fundamental APM parameters to investigate the SB of galaxies.

Additionally, there are two other APM parameters that are related to the profile of galaxies. Both of them are density weighted parameters. One is σ^2 , defined as

$$\sigma^2 = \frac{\sum_{D_{\text{obj}} \geq t} (x^2 + y^2) D_{\text{obj}}(x, y)}{I_{\text{iso}}} \quad (7)$$

where, $D_{\text{obj}}(x, y)$ is the density at location x and y relative to the image centroid. Theoretically, σ^2 , together with A_{iso} can constrain the SB profile of the image, and judge whether it is best fit by a Gaussian, or exponential, or even an $r^{1/4}$ profile. Unfortunately, in practice this is not possible, because σ^2 changes by only about 10% between these three profiles, and this is the same order as the observational error in σ^2 (see Section 5). Additionally, σ^2 can be seriously affected by other factors, such as the ellipticity and substructure of the image, and any other asymmetry of the profile which will tend to increase σ^2 . This means that the measurement of σ^2 is not as robust as A_{iso} or I_{iso} , and so we do not use σ^2 in the measurement of SB in this paper. In Section 5.2, we consider the distribution of σ^2 for bright galaxies which have a large image and hence a smaller error in σ^2 , and show that an exponential profile is actually a reasonable approximation to the SB profile of most galaxies.

Another useful parameter is the ellipticity of the image, which is derived from density-weighted second moments. This can be easily converted to the apparent axial ratio of the APM image (Maddox et al. 1990a; Lambas et al. 1992),

$$e = \left(\frac{b}{a} \right)_{\text{apparent}}. \quad (8)$$

On the assumption that the areal profiles of an APM image have similar shapes, then e is independent of other profile parameters, and will not affect the measurement of SB. However, e will affect the estimation of σ^2 as discussed in Section 5.2.

3.2 Modelling the SB profile of galaxies

If the image of a galaxy is represented by a circularly-symmetric pure exponential surface brightness profile,

$$p(r) = p_0 \exp(-r/r_0). \quad (9)$$

The central peak value p_0 , and the characteristic size r_0 fully describe the image. In this case, r_0 is the exponential scale

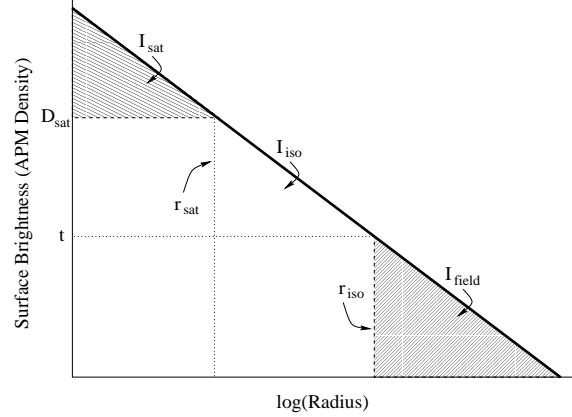


Figure 1. Schematic representation of various quantities used in our estimation of μ_0 . The solid line represents the galaxy SB profile as a function of radius. D_{sat} is the maximum measured APM density, and r_{sat} is the radius where this density is reached. The shaded area above D_{sat} represents the flux lost due to the saturation, I_{sat} . The isophotal measurement threshold is shown by the horizontal dotted line, labeled t , and r_{iso} is the isophotal radius. The shaded area to the right of r_{iso} represents the flux lost due to the isophotal threshold, I_{field} . The unshaded area below the solid line is the observed isophotal flux, I_{iso} .

length. The total luminosity of the image, I_{tot} , is simply the integral of $p(r)$. The integration can be divided into three parts which contribute to I_{tot} ,

$$I_{\text{tot}} = I_{\text{sat}} + I_{\text{iso}} + I_{\text{field}}, \quad (10)$$

where I_{sat} , I_{iso} and I_{field} represent the flux lost due to saturation, the observed flux and the unobserved flux beyond the isophotal size of the galaxy respectively. These can be written as:

$$I_{\text{sat}} = 2\pi \int_0^{r_{\text{sat}}} p(r)rdr - 2\pi r_{\text{sat}}^2 D_{\text{sat}}; \quad (11)$$

$$I_{\text{iso}} = 2\pi \int_{r_{\text{sat}}}^{r_{\text{iso}}} p(r)rdr + 2\pi r_{\text{sat}}^2 D_{\text{sat}}; \quad (12)$$

and

$$I_{\text{field}} = 2\pi \int_{r_{\text{iso}}}^{\infty} p(r)rdr, \quad (13)$$

where

$$r_{\text{iso}} = \sqrt{A_{\text{iso}}/\pi} = r_0 \ln(p_0/t) \quad (14)$$

denotes the radius corresponding to the isophotal area for circular images and

$$r_{\text{sat}} = r_0 \ln(p_0/D_{\text{sat}}) \quad (15)$$

denotes the radius corresponding to the saturated area for circular images. These quantities are illustrated schematically in Figure 1. Of these three parts, I_{iso} is the only directly observed quantity, and is given by $\sum_{D_{\text{obj}} \geq t} D_{\text{obj}}$ (eq. 3). The measured values of I_{iso} and A_{iso} can be used together with eq.(14) and eq.(15) to find the parameters p_0 and r_0 . The resulting equations are not soluble analytically, but are simple to solve numerically. The actual procedure that we adopt is as follows: take an initial value of (p'_0, r'_0) ; calculate the $(A'_{\text{iso}}, I'_{\text{iso}})$ from eq.(12), eq.(14) and eq.(15). Then compare

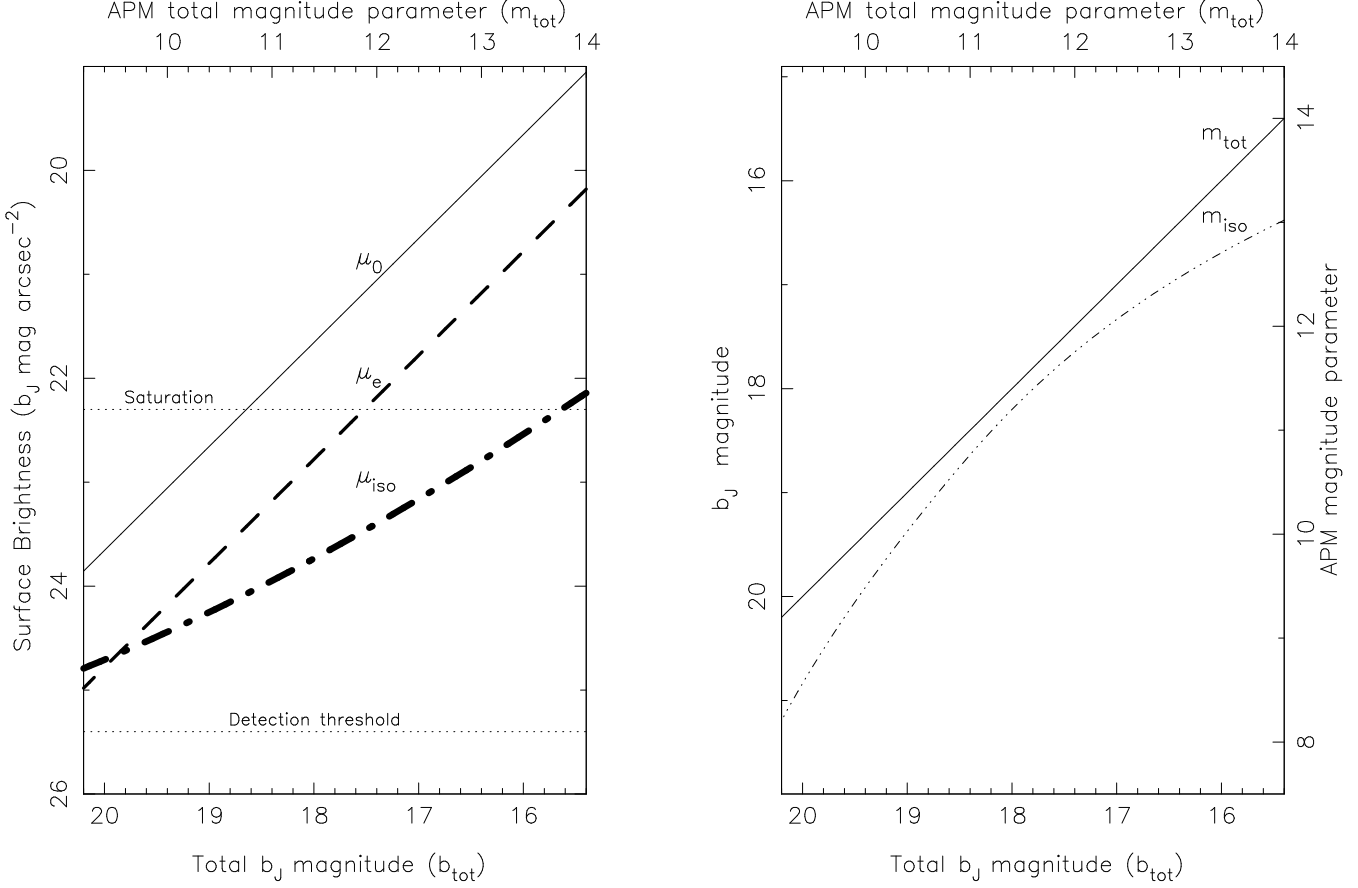


Figure 2. (a) *Left:* Simulated surface brightness estimates, μ_0 (central SB), μ_e (mean SB within r_e) and μ_{iso} (mean SB within the detection isophote, eq. (18)) for an isophote $t = 25.4$ mag arcsec $^{-2}$ as a function of total magnitude, b_{tot} , for circularly-symmetric exponential profile galaxies. The value of r_0 is fixed in this example at 2.15 arcsec (a typical value for the scale length), and the threshold and saturation value are set as 12 and 200 APM density units per pixel above the sky level. (b) *Right:* The isophotal magnitude, m_{iso} , (dashed line) as a function of total magnitude, m_{tot} , for circularly-symmetric exponential profile galaxies with $r_0 = 2.15$ arcsec, illustrating the effects of the isophotal threshold and saturation. The total magnitude relation is shown (as a solid line) for comparison. Results are shown for both APM magnitude parameters (equations (4) and (19)) and for conventional magnitudes.

with the observational APM parameters (A_{iso} , I_{iso}), and calculate a feedback of $(\Delta p'_0, \Delta r'_0)$. Several iterations will lead to the final stable result of (p_0, r_0) . The analysis can be adapted to non-circular images by assuming concentric elliptical isophotes and using the APM ellipticity.

The effects of seeing can also be included in this iterative process, but for most galaxies the correction is less than 0.1 mag. Our estimates of p_0 are based on I_{iso} and A_{iso} , and for images larger than about 100 pixels these measurements are not sensitive to the seeing.

3.3 Surface Brightness

The pair of parameters (p_0, r_0) entirely describes the exponential profile of circularly-symmetric images, so they can be used to infer the value of any other characteristic SB parameter for such a galaxy. In particular we can define the central SB in units of magnitudes per unit area,

$$\mu_0 = Z - 2.5 \log_{10}(p_0) \quad (16)$$

where Z is the zero-point for that particular UKST plate. We can also define an effective SB,

$$\mu_e = \mu_0 + C \quad (17)$$

where the constant C depends on the exact definition of the effective SB. It can also be useful to define an effective radius, r_e , which is the radius containing half the light of the galaxy. This is related to the scale size by $r_e = 1.678 r_0$ for a circularly-symmetric image with an exponential light profile. For the SB at r_e , the constant is $C = 1.822$, and for the mean SB within r_e , $C = 1.124$. Also the average SB within the isophotal area (for the APM scans of UKST blue plates this isophote is ≈ 25 b_J mag arcsec $^{-2}$) can be written as

$$\mu_{\text{iso}} = Z - 2.5 \log_{10} \left(\frac{I_{\text{iso}}}{A_{\text{iso}}} \right) \quad (18)$$

where A_{iso} and I_{iso} are the corresponding isophotal size and brightness, derived directly from eq.(9). Additionally, one can also calculate the ‘total APM magnitude’ from I_{tot} ,

$$m_{\text{tot}} = +2.5 \log_{10}(I_{\text{tot}}) = +2.5 \log_{10}(2\pi p_0 r_0^2), \quad (19)$$

for circular images. This is related to the conventional total magnitude of the image, which is given by

$$b_{\text{tot}} = Z - 2.5 \log_{10}(I_{\text{tot}}) = Z - 2.5 \log_{10}(2\pi p_0 r_0^2) \quad (20)$$

where Z is the magnitude zero-point.

The relationship between these three SB measures can be seen in Figure 2. In this Figure, we fix the value of r_0 to illustrate the dependencies between these SB parameters, giving r_0 a value of 2.15 arcsec, chosen to be fairly typical of the APM sample. Though the different SB measures are all derived from the same set of (p_0, r_0) data, we see in Figure 2a that some galaxies can show much larger differences between μ_{iso} and either μ_0 or μ_e than other galaxies. Figure 2b presents the isophotal magnitude, labelled m_{iso} , as a function of the total magnitude for the same value of r_0 . This is shown for both the standard magnitude and for the APM magnitude parameters of equations (4) and (19). m_{iso} can be significantly fainter than m_{tot} , at both high and low SB. At high SB (bright total magnitude), the flux I_{sat} is lost because of the emulsion saturation; at low SB (faint total magnitude) the flux I_{field} is missed because of the isophotal limit. This also provides a rough estimate of how much μ_0 will be underestimated if these two parts of missing flux are not accounted for. The effect of saturation and isophotal threshold on the magnitude is shown explicitly in Figure 3(a). As mentioned in Section 3.1, bright galaxies may be saturated over a large fraction of the image. This can be seen quantitatively in Figure 3(b), which shows the ratio of isophotal radius, r_{iso} , and saturation radius, r_{sat} , to the scale length, r_0 as a function of total magnitude.

As described above, this approach only provides a rough measurement of the SB of galaxies. It does not use the real profile of different types of galaxies, which may be different from an exponential disk. It also neglects any internal structures, such as arms, bars or a central bulge. Also, although we have rejected images that are most likely to be merged pairs, the automated image classification is not perfect, and there is a residual contamination of about 5-10% of merged images, whose profiles will not be well represented by our simple model.

Although for any individual galaxy our SB measurement is unlikely to be very accurate, it is helpful to constrain the shape of any given profile and it does allow us to make general comparisons of galaxy SB within the whole sample. Theoretically, this approach is suitable for any other profile which is specified by only two parameters, such as a Gaussian profile,

$$p(r) = p_0 \exp(-(r/r_0)^2) \quad (21)$$

or an $r^{1/4}$ law profile,

$$p(r) = p_0 \exp(-(r/r_0)^{1/4}). \quad (22)$$

Without any other effective observational constraints on the profile shape an exponential profile is the most reasonable choice since it is a good representation for a majority of galaxies. As discussed in Section 5.2, we find that σ^2 as defined in eq.(7) is not very effective in distinguishing between different profiles. Additionally, the exponential profile has been a popular choice in earlier work, so it allows us to compare with other results. So, in this paper, we continue our

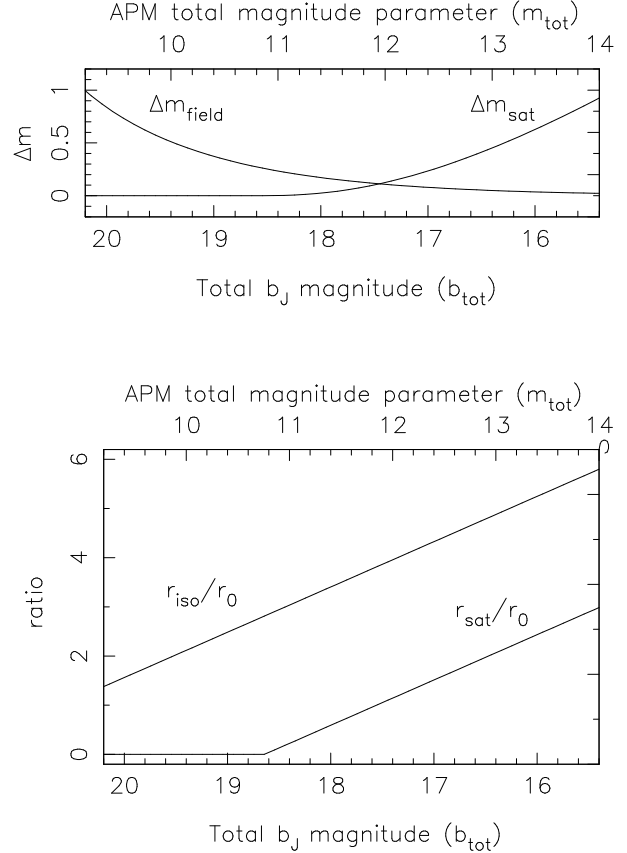


Figure 3. (a) *Top*: The change in total magnitude due to the isophotal threshold, Δm_{field} , and saturation, Δm_{sat} , as a function of total magnitude. (b) *Bottom*: The ratio of isophotal radius, r_{iso} , and saturation radius, r_{sat} , to the scale length, r_0 as a function of total magnitude. The value of r_0 is fixed at 2.15 arcsec, as for Figure 2.

analysis and discussions under the assumption that galaxies have an exponential SB profile.

Note that these estimates are in terms of the “APM” SB, which is based on APM density measurements. They are directly related to true SB only if there is a linear relationship between the real flux and the APM density (eq.1). Clearly the emulsion saturation violates this assumption, and CCD observations show that it is not exactly linear below saturation (Cawson et al. 1987). Our fitting technique approximates the saturation as a simple maximum APM density, and ignores any non-linearity below the saturation density. This non-linearity will not strongly influence the ordering of galaxies as a function of their SB, but more accurate measurements would have to allow for this factor. Furthermore, if the intrinsic SB is required for a particular analysis instead of the apparent SB, then the K-correction, cosmological dimming, and the correction of the apparent ellipticity of disk galaxies should also be taken into account.

4 FIELD CORRECTION AND OVERALL PLATE MATCHING

To provide a uniform sample of SB measurements over the whole APM galaxy survey area, we make two further sys-

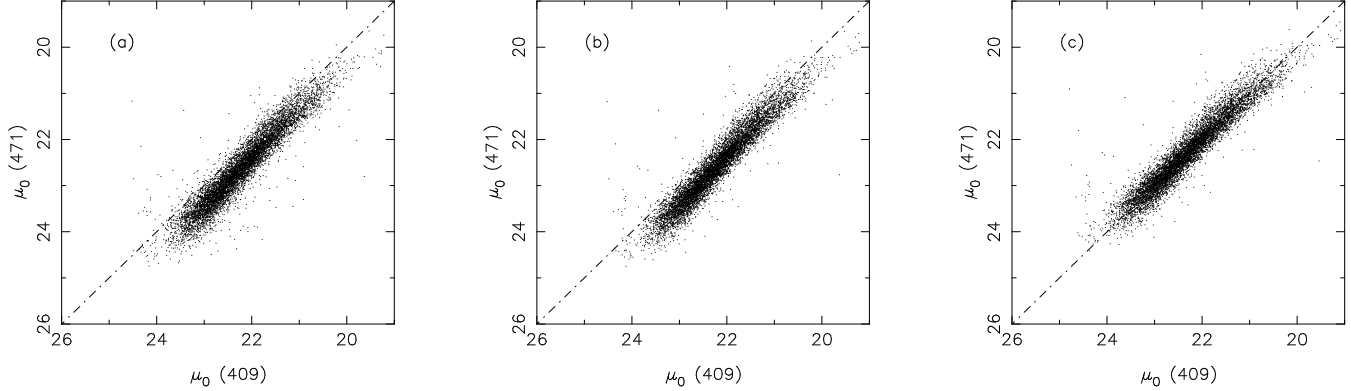


Figure 5. Comparisons of the b_J central surface brightness of galaxies within the overlapping region of UKST fields F409 and F471 (a) before any correction; (b) after field correction (Section 4.1); (c) after further calibration of the magnitude zero-points by matching results for galaxies in overlapping regions of UKST plates (as in Section 4.2). The *rms* scatter in the differences are in turn 0.27, 0.25, 0.25 mag arcsec⁻². The dashed line in each panel shows the line $\mu_0(409) = \mu_0(471)$.

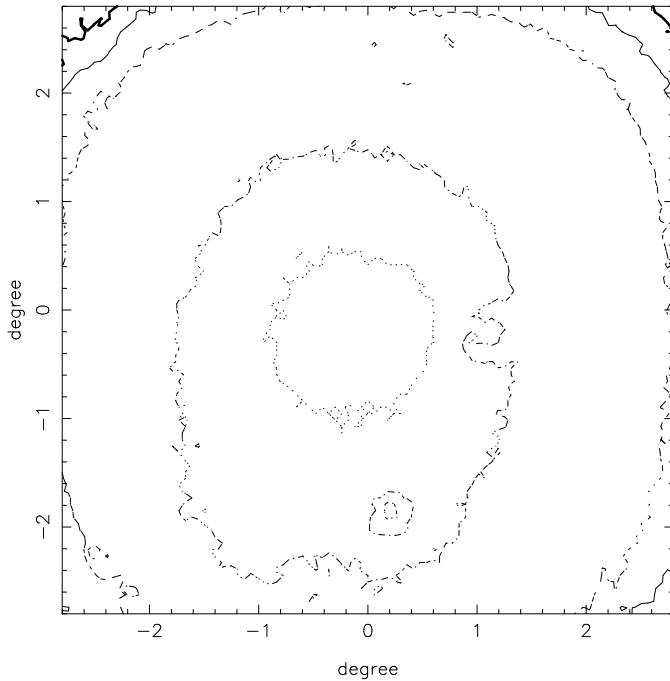


Figure 4. A contour plot of the field correction values, averaged over 185 plates. The dotted line shows $\Delta\mu_1 = -0.015$ mag arcsec⁻², the dash-dot line 0.0 mag, the dashed line 0.1 mag, the solid line 0.2 mag and the thick solid line 0.3 mag

tematic corrections. First, we correct for the field response function to make the different parts of each UKST plate consistent from the central region to the edge. Then, we make an overall photometric zero-point adjustment to each plate, to give a uniform sample over the whole survey area.

4.1 Field response corrections

The variation in the response function across the field of each plate is caused by two main factors. One is the geometrical vignetting of the optical system of the telescope (UKST), that reduces the effective transmission off its axis. A theoretical analysis (Dawe & Metcalfe 1982) shows the transmis-

sion is very flat for images closer than 2.5° from the center of a plate, but quickly falls to $\approx 80\%$ of the central value at 4° off axis. This reduction is same for each plate. Another loss in sensitivity is caused by the differences in the chemical desensitization at different parts of the UKST survey plates. For most of the survey plates, the original plate holder has an air gap between the plate and the filter, and the greater air circulation near the plate edges caused greater desensitization of the hypersensitized III-aJ emulsion. This effect causes a multiplicative reduction in the measured flux, which is quite similar to the geometrical vignetting, but the pattern actually varies for different plates, because the local weather conditions during individual observations were significantly different.

Both of these effects can be considered as a change in the relation between APM densities and true flux. If two objects have same flux, f_{obj} , but are located at different positions on a plate, then the geometrical vignetting and the different desensitization lead to different observed APM densities D_{obj} via eq.(2). The constant β is essentially the fog level of the emulsion, which is constant, so the loss in sensitivity means that the slope α is not a constant across the plate. It is a function of position in the field, being reduced by the geometrical vignetting and emulsion desensitization from centre to the edge. Thus, both these effects can be considered as variations in α .

Fortunately, α is only a function of position in the field, and does not depend on the specific properties of an image. Therefore, the correction process of Maddox et al. (1990b), which was devised to correct the total magnitude of images, can be simply applied here to correct the SB of galaxies. According to eq. (8) of Maddox et al. (1990b), the correction to the total APM magnitude is

$$\Delta m_1 = 2.5 \log_{10} \left(\frac{\alpha_1}{\alpha_0} \right) \quad (23)$$

where the subscript 0 denotes the centre of a plate and the subscript 1 denotes the particular position of an object. According to the relationship between the central SB and the total APM magnitude of eqs. (16) and (19), we can see that

μ_0 will need the same correction as m_{tot} :

$$\Delta\mu_1 = -2.5 \log_{10} \left(\frac{\alpha_1}{\alpha_0} \right). \quad (24)$$

The value of $\Delta\mu_1$ is determined individually for each galaxy by estimating the APM sky density in the surrounding 10 arc minutes. The apparent variation in sky density is converted to an effective change in α using an empirical relation which was chosen to ensure that the number density of galaxies is uniform when averaged over many UKS plates. This correction will be generally applicable for other SB measurements, except for the mean isophotal surface brightness, μ_{iso} . Since the threshold t is fixed in terms of observed APM density, the actual threshold isophote varies over each field and a more complex correction would be required to ensure that μ_{iso} is uniform.

Most survey galaxies are located within the central 3° radius of a UKST plate, and so the correction is very small, typically ≤ 0.1 magnitude. For galaxies outside this region the correction can increase up to 0.4 mag. See figure 4 for the pattern of averaged $\Delta\mu_1$ of field correction. See the figures of Maddox et. al (1990b) for further details.

Figures 5(a) to (b) show that the field correction slightly reduces the *rms* difference between the SB measurements for those galaxies imaged on two independent plates. F409 and F471 are a pair of contiguous plates with quite a large overlapping area, and there is a total of 7960 identified galaxies with measurements from both the plates. For quite a few of these galaxies, the distance from the centre of one of the plates can be large, which means that uncorrected values of $\Delta\mu_0$ can be quite large. Figure 5 (a) plots the μ_0 before field correction and (b) after it. The *rms* scatter in these two plots is reduced from 0.27 to 0.25 mag. This improvement suggests that the *rms* $\Delta\mu_0$ from the field correction is $\simeq 0.1$.

4.2 Matching calibrations in plate overlaps over the whole survey

Variations in the emulsion sensitivity and observing conditions mean that each UKST survey plate has a different photometric zero-point. To produce a uniform set of galaxy SB estimates, we need to adjust the zero-point of each plate to force a match between galaxies in overlapping regions. In the APM survey paper II, Maddox et al. (1990b) described a scheme to match the APM total magnitudes over the survey. In this paper we apply a similar procedure to match our SB estimates.

The matching procedure uses the fact that each plate covers an area of sky that overlaps with its neighbours, so there are many galaxies that have independent measurements from two neighbouring plates. For a particular overlap the mean difference between the two measurements gives an estimate of the difference between the zero-points of the two plates. Taking all overlaps together we can find the set of plate zero-points which is most consistent with these plate-to-plate offsets.

The main difference for this paper is that a galaxy SB profile is determined by two parameters (p_0 , r_0) as described in Section 3, and so both parameters must be matched. In principle, we could choose to match any two independent parameters derived from these two, but for simplicity we choose μ_0 and b_{tot} . They are related to p_0 and r_0 through

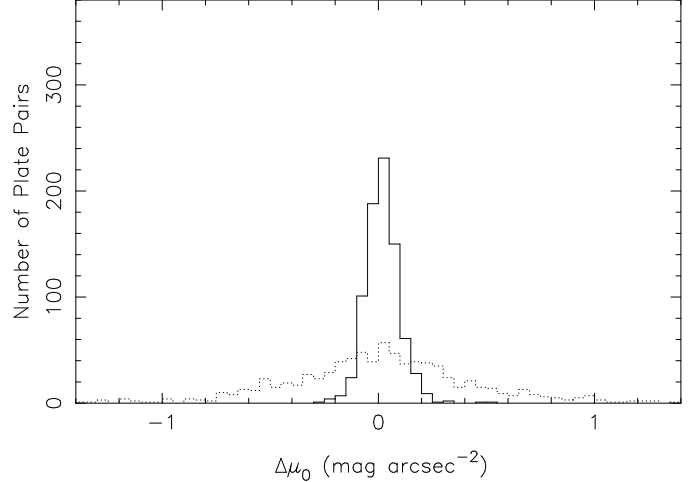


Figure 6. The frequency distribution of offsets in μ_0 for galaxies in 809 overlapping fields. The dotted histogram shows the results before matching, with $\sigma = 0.43$ mag arcsec $^{-2}$; The solid line shows the distribution after matching, with $\sigma = 0.08$ mag arcsec $^{-2}$.

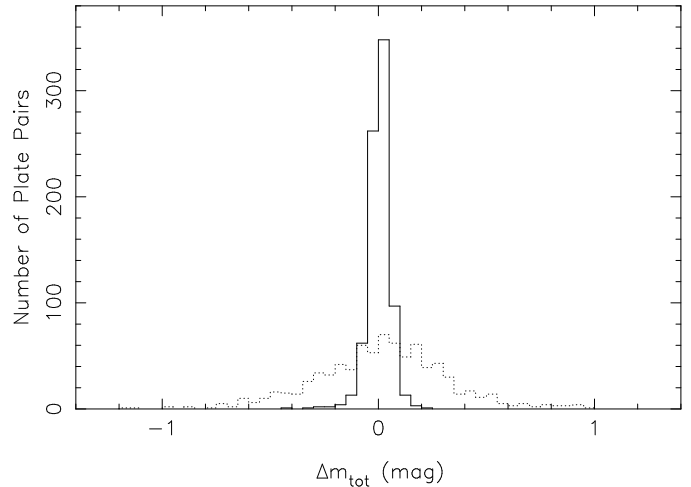


Figure 7. The frequency distribution of offsets in m_{tot} for galaxies in 809 overlapping fields. The dotted histogram shows the results before matching, with $\sigma = 0.31$ mag; The solid line shows the distribution after matching, with $\sigma = 0.05$ mag.

eqs. (16) and (20), while the zero-point in eq. (16) represents the overall corrected uniform zero-point. Since we have assumed exponential profiles in this analysis, the magnitude zero-points are not the same as the Gaussian total magnitudes that were applicable to galaxies near the plate limit, as used in previous work on the APM galaxy survey.

Images were matched in the overlaps of every pair of plates with centres closer than 7° . For the 269 plates in the south galactic cap, this gives 809 distinct overlaps with an average of 1405 galaxies brighter than $b_J = 20.5$ in each overlap. To allow for non-linearities which introduce a non-unit slope in the APM magnitude and SB measurements we used a linear fit to $(\mu_i - \mu_j)$ vs $(\mu_i + \mu_j)/2$. Before matching, the variance in zero-point for the different UKST survey plates is very large, as can be seen in the offset of μ_0 for galaxies in the overlapping plate pairs. The distribution of

offsets $\bar{\mu}_1 - \bar{\mu}_2$ for all 809 overlaps, is shown in Figure 6, and the *rms* scatter is 0.43 mag. After matching, this value is reduced to 0.08 mag. As shown in Figure 7, similar reduction in scatter is seen for m_{tot} , where the *rms* before matching is 0.31 mag, and after matching is 0.05 mag.

For different plates, the zero-point corrections for μ_0 and m_{tot} are well correlated, but not exactly the same. The scatter about the correlation is caused by the different seeing on different plates, which leads to a different apparent r_0 . The matching process has effectively given r_0 for galaxies on each individual plate a systematic correction to a common “zero-point”.

4.3 Error estimation

For an individual galaxy, the deviation of the actual SB profile from an exponential profile is likely to be the main source of error in the SB estimate, but this effect is beyond the scope of this paper. If we assume a given profile, then we can discuss the “intrinsic” error in the APM SB caused by the observational errors in $(I_{\text{iso}}, A_{\text{iso}})$.

The errors in $(I_{\text{iso}}, A_{\text{iso}})$ come from a complex combination of sources which we consider in two main categories. First is the observing process, which includes a mixture of weather conditions and instrumental effects, including the residual calibration differences between the survey plates that are not corrected by the field correction function and overall plate matching. This category also includes photon noise. Second are the errors from the APM scan itself. These errors can be estimated directly from repeat scans of selected plates. For I_{iso} we find this source contributes only about 0.04 mag uncertainty, and for A_{iso} we find about 5%. These errors could be analytically transformed to μ_0 following a standard propagation of errors procedure, but even if the resulting uncertainty in μ_0 is slightly larger, it will be negligible compared to the observational errors.

The overlapping areas of neighbouring plates provide a direct opportunity to estimate the combined errors in our SB estimates. Figure 5(c) shows the residual errors for the overlapping field of F409 and F471, after applying the field correction and the overall matching correction, and it can be seen that there is still an *rms* scatter of about 0.25 mag between the two independent measurements for each galaxy. This implies the error in each μ_0 will be $\simeq 0.18$ mag. We have calculated the *rms* scatter for each one of the 809 plate overlaps, independently, and show the frequency distribution of these *rms* values in Figure 8. For most of these overlaps, the *rms* of $\Delta\mu_0$ is less than 0.3 mag, and the mode is at 0.21 mag, corresponding to a typical uncertainty of 0.15 mag for an individual SB measurement.

If we consider all of the plate overlaps as a whole, the *rms* $\Delta\mu_0$ over all 1,282,600 galaxy pairs is 0.23 mag, so the overall uncertainty for an individual SB measurement has an *rms* of 0.16. This value includes both the random error on each SB measurement, and the *rms* residual difference between the zero-points for all plates after applying the matching corrections. The difference between this *rms*, and the *rms* within each overlap suggests that the residual error in the zero-point matching has an *rms* of 0.07 mag per plate, consistent with the overlap residuals.

Additionally, we have considered the error as a function of μ_0 . Table 1 lists the *rms* difference between the μ_0

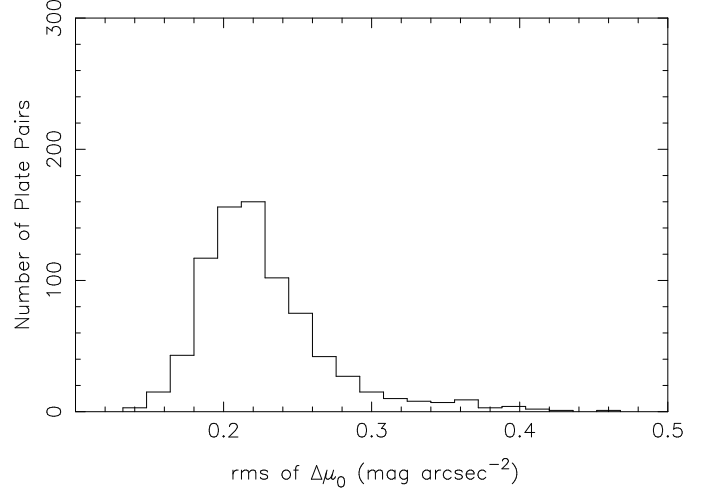


Figure 8. Frequency distribution of scatters (*rms*) of $\Delta\mu_0$ of galaxy pairs for 809 overlapping fields.

Table 1. The *rms* uncertainty in μ_0 for galaxy pairs with different central surface brightnesses

μ_0 (mag arcsec $^{-2}$)	no. of galaxy pairs	<i>rms</i> of $\Delta\mu_0/\sqrt{2}$
24.5 \sim 23.5	40832	0.22
24.0 \sim 23.0	202094	0.19
23.5 \sim 22.5	480355	0.17
23.0 \sim 22.0	639704	0.16
22.5 \sim 21.5	564329	0.16
22.0 \sim 21.0	373165	0.16
21.5 \sim 20.5	181962	0.18
21.0 \sim 20.0	62253	0.21
20.5 \sim 19.5	14258	0.23

measurements in overlaps for a series of μ_0 ranges. Galaxies with μ_0 about 21.0 \sim 22.0 mag have the smallest error at 0.16 mag. At both low and high surface brightness the error increases up to $\simeq 0.23$. This tendency could also be seen in Figure 5(c). The reason for the increased error is that μ_0 depends on the profile of a galaxy (see Section 5.2), and when we estimate the total intensity of the galaxy, I_{tot} (eqs. (10) to (13)), only I_{iso} is directly constrained by the observational data, while I_{field} and I_{sat} , the other two contributions to I_{tot} , involve extrapolations that are more extreme at low or high SB.

So in summary, the overall “intrinsic” uncertainty in μ_0 including measurement errors, and zero-point errors is typically 0.2 mag. Comparing galaxies measured on one plate, the relative uncertainty is about 0.16 (also see the next subsection).

4.4 Galaxy surface density and mean μ_0

After applying the corrections to the individual plate data, we should be able to define galaxy catalogues selected with uniform SB criteria. We can make a simple test of the uniformity of the sample by calculating the mean SB for galaxies on each plate. Cosmic structure will introduce some intrinsic

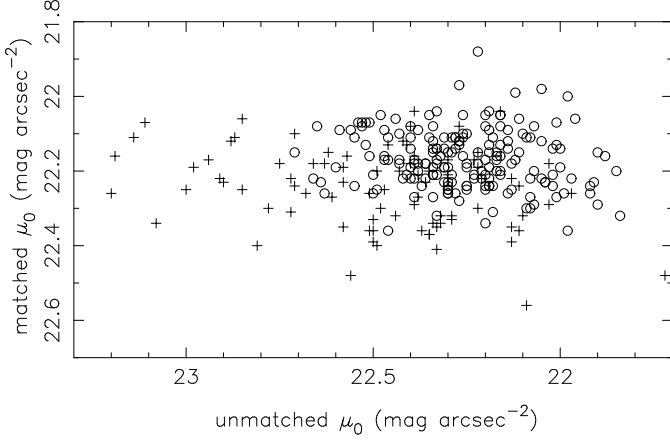


Figure 9. The distribution of mean μ_0 for all plates in the survey. Circles show fields where the declination of the centre is $\leq -20^\circ$, and crosses show fields where the declination of the centre is $> -20^\circ$.

variation in the mean SB in different directions on the sky, but this is likely to be small; indeed the variation in galaxy numbers from plate to plate at $b_J = 20$ is only 12% (Maddox, Efstathiou & Sutherland 1996). Figure 9 shows a plot of the mean μ_0 for each plate in the survey, before and after applying the matching corrections. Using all fields, the *rms* scatter before correction is 0.25 mag, and after correction it reduces to 0.095 mag. However, it is clear that fields centred with declination $> -20^\circ$ have a larger scatter, even after correction. This is partly due to the fact that the scanned plates with declination $> -20^\circ$ are a rather heterogeneous mix of original plates and non-survey plate copies, and partly due to the significantly large galactic extinction in this part of sky (see Schlegel, Finkbeiner & Davis 1998). In principle it should be possible to correct these problems, but for simplicity we have simply excluded the fields with declination $> -20^\circ$ in the subsequent analysis.

A further simple check on the uniformity is to compare the average number of galaxies per plate for SB selected samples. Figure 10 shows the distribution of galaxies on the sky for three subsamples selected on SB from high to low SB respectively. The ranges in μ_0 were chosen to give samples with roughly the same number of galaxies in each subsample. Note that the high and low SB samples are selected from the tails of the SB distribution (see Section 5.1) and so are most sensitive to errors in the plate matching.

For the 185 plates there are no plates which show a clearly discrepant number of galaxies, suggesting that our matching procedure does indeed produce a uniform set of SB measurements. This improvement can also be seen in figure 11, which plots the numbers of galaxies in each plate for these three subsamples before and after matching correction. After matching, the fractional *rms* scatters in the number of galaxies on each plate are 0.27, 0.13, 0.17 respectively for the three samples. These are close to what is expected for randomly selected $5^\circ \times 5^\circ$ patches of sky.

The higher *rms* for the high SB sample reflects the higher clustering amplitude of high SB galaxies, which is clearly apparent in Figure 10. We plan to quantify these differences in clustering in a future paper.

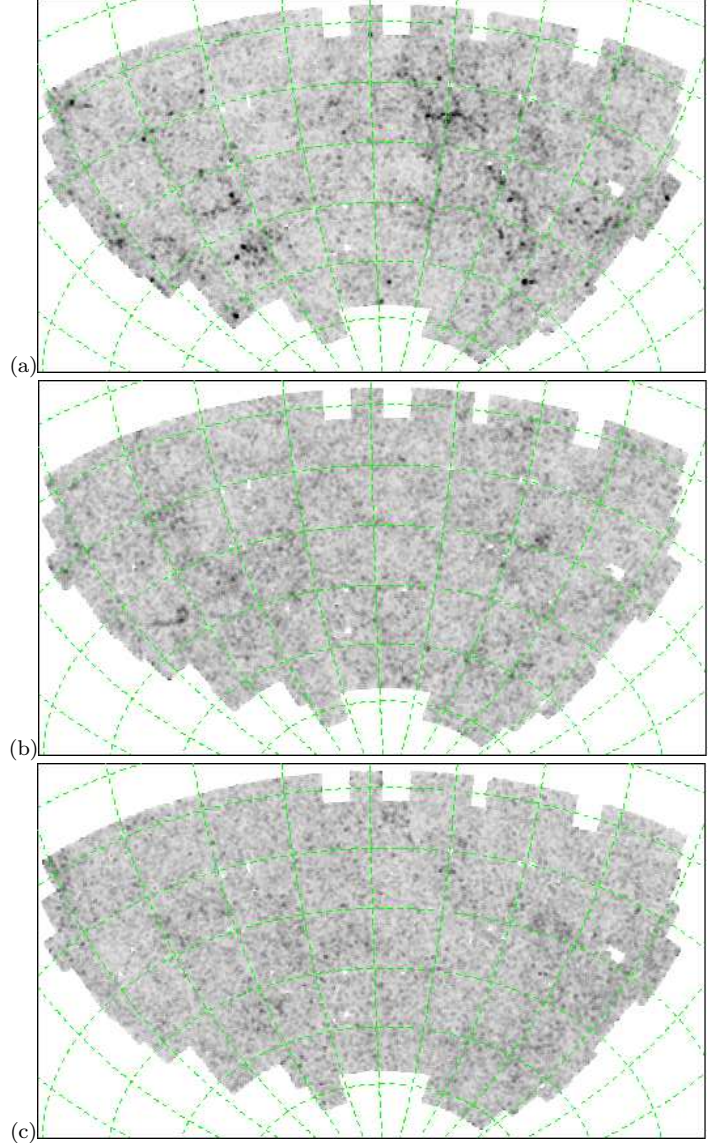


Figure 10. The distribution of SB selected subsamples of galaxies projected on the sky: (a) $20.5 < \mu_0 < 21.2$ b_J mag arcsec $^{-2}$; (b) $22.0 < \mu_0 < 22.2$ b_J mag arcsec $^{-2}$; (c) $23.0 < \mu_0 < 24.5$ b_J mag arcsec $^{-2}$. Each panel shows a greyscale map shaded according to the surface density of galaxies in $14' \times 14'$ cells over the SGP. White represents 0 galaxies per cell, and black represents 4 times the mean surface density. The dashed lines show right ascension and declination.

4.5 Checking the APM results and photometric calibration with deeper CCD data

It is important to test the accuracy of the APM surface photometry, particularly the photometric calibration, through a comparison with well-calibrated higher-resolution CCD data. To this end, new CCD surface photometry has been performed on faint ($b_J \simeq 18$ to 22 mag) galaxies in the region around the Hubble Deep Field South (HDF-S), which lies in the area of the available APM data (at galactic coordinates $(l, b) = (328^\circ, -49^\circ)$). Much well-calibrated public imaging data are available around the HDF-S, and ground-based HDF-S CCD observations cover a sufficient area to provide the numbers of galaxies required for these tests. The

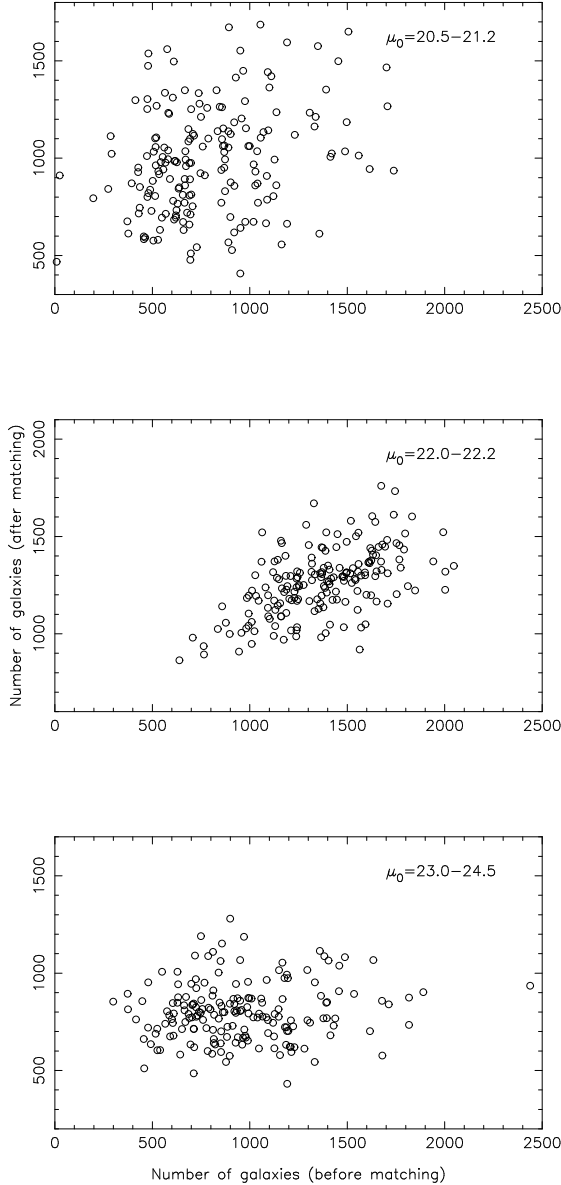


Figure 11. The number of SB selected subsamples of galaxies per UKST survey plate's central $5^\circ \times 5^\circ$ region, before and after matching correction. Their *rms* scatters, normalized by their average numbers of galaxies, are 0.40, 0.20, 0.35 separately before matching and are reduced to 0.29, 0.13, 0.19 after it.

Goddard Space Flight Center HDF-S public data (Teplitz et al. 2001; Palunas et al. 2000) were selected for the task because they combine a large image area, standard broadband photometric passbands and good photometric calibrations. The Goddard HDF-S data were recorded with the Big Throughput Camera on the 4-metre Blanco telescope at the Cerro-Tololo Inter-American Observatory (Wittman et al. 1998) and cover a 47 arcmin by 46 arcmin area. An independent measurement found that the seeing of the blue data was 1.7 arcsec in the central 15 arcmin by 15 arcmin region; although not good, this is comparable to or better than the photographic APM data. Pixels were 0.43 arcsec in width.

We measured the SB profiles of galaxies in this region through the following steps. Firstly, images were detected in

the B-band CCD data using the SExtractor package (Bertin 1998; Bertin & Arnouts 1996). This provided image centroid positions, ellipticities and orientations. For each galaxy image, mean surface brightnesses were computed in a series of concentric elliptical annuli defined by these SExtractor image parameters. Then the surface brightness was plotted against semi-major axis for each image and an exponential light profile fitted, defining the range in semi-major axis for these fits by visual inspection. Care was taken to avoid fitting to the core of the image where seeing effects were significant. This provided a central surface brightness and exponential scale length for each selected galaxy. Finally, the surface brightness results were transformed from the instrumental blue magnitude system to the photographic b_J system using the Goddard HDF-S transformation and the standard B to b_J equation of Blair & Gilmore (1982). This used colours measured within identical elliptical apertures in the B and V data. The overall uncertainty in the individual central surface brightness measurements is about 0.1 mag.

An independent check of these results was made using other public ground-based HDF-S data. SExtractor total magnitudes were computed using the Anglo-Australian Observatory public CCD observations for the region immediately around the WFPC2 field. These were transformed to the b_J band and compared with the total magnitudes under the fitted exponential profiles derived from the Goddard HDF-S data. Six galaxies with Goddard photometry were identified in the AAO field. The difference in the total magnitudes was $+0.032 \pm 0.030$ mag, confirming the validity of the results obtained from the Goddard public data. The surface photometry from the Goddard data can therefore be used to check the APM photographic results.

The HDF-S CCD surface photometry gave central surface brightnesses μ_0 and scale lengths r_0 for a large sample of galaxies with $b_J = 17.5$ to 22 for which the exponential profile was judged to be an adequate fit. Of this sample, 24 objects appeared in the APM Galaxy Catalogue. Of these 24, two galaxies were rejected from further consideration because their angular sizes were so small (isophotal areas smaller than 100 pixels) that seeing was likely to affect appreciably the results from the APM data. This left 22 galaxies in the region around the HDF-S that had surface photometry both from the APM data and from the CCD observations. These galaxies were used to test the reliability of the surface brightness results derived from the APM data.

Figure 12 shows the relationship between the CCD μ_0 and our APM measurements. The *rms* scatter is 0.29 mag arcsec $^{-2}$, and the difference in their zero-points is 0.26 mag arcsec $^{-2}$. This dispersion is larger than expected from simply adding the uncertainty of 0.18 in the APM measurements in quadrature with 0.1 from the CCD measurements. The extra scatter is probably due to the fact that we have not corrected the non-linear correspondence between flux and the emulsion density of the survey plates. Note also that nearly all of the galaxies in this sample have $\mu_0 < 22$ mag arcsec $^{-2}$, which is brighter than the saturation level of the UKST emulsion and thus the APM measurements depend on extrapolated galaxy profiles.

The scatter could be reduced by restricting the range in radius used to fit the CCD data so that it matches more closely the range available in the APM data. However, this would not be a true representation of the uncertainties in

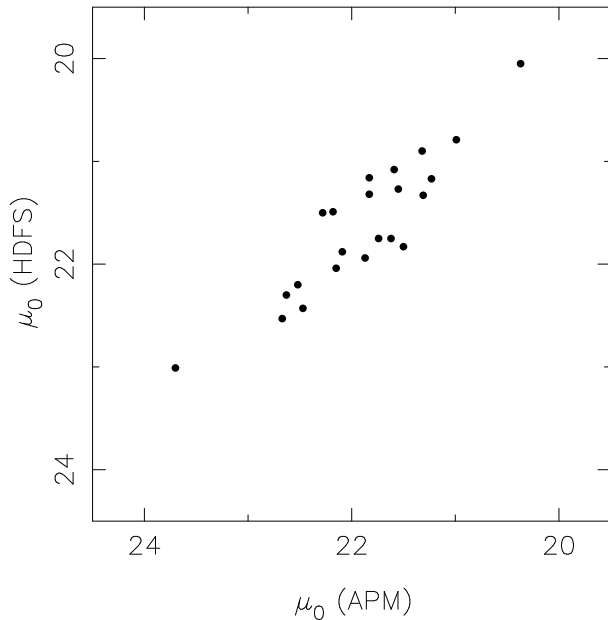


Figure 12. Comparison of central surface brightness of HDF-S and this paper. The *rms* scatter is $0.29 \text{ mag arcsec}^{-2}$.

the APM SB estimates. We want to compare the APM results with results from CCD surface photometry that have been obtained using standard surface photometry methods. Note that there will also be systematic biases correlated with morphological type. Since we have assumed an exponential profile, a galaxy with an $r^{1/4}$ profile will not be well represented by our model (see Section 5.2).

In summary, although the APM measurements have relatively large uncertainties, they are adequate to classify galaxies into broad surface brightness categories.

4.6 Comparison with other SB measurements of UKST survey plates

Morshidi-Esslinger et al. (1999, hereafter MDS) made a survey of a substantial number of UKST survey plates in the south galactic cap in an attempt to identify LSBGs with large angular size. They used the APM to measure profiles of nearly 3000 LSBGs and estimated the central surface brightness by extrapolating the best fit exponential profile. Their SB estimates are based on the same original plates as our data, and they use the same scanning machine. They also make the same assumption of exponential galaxy profiles, so the MDS survey is not a completely independent data set. Nevertheless it provides a useful comparison for our estimates.

There are two main differences between our measurements and those of MDS. First, they fitted exponential profiles to up to 8 isophotal areas A_0, A_1, \dots, A_7 – see the details in Maddox et al. (1990a) and MDS (1999) – to solve for the (p_0, r_0) parameters, whereas we used only A_0 to calculate these values. The second difference is in the calibration procedure. MDS’s calibration of SB depends on zero-points for total magnitudes from other works for fields where this is available, and uses the magnitudes of stars in plate overlaps for fields with no external calibration. Our calibration de-

pends mainly on matching μ_0 directly for the galaxies plate overlaps, with an overall calibration from external photometry.

Figure 13 compares our estimates of μ_0 with 2185 MDS galaxies that can be identified in our sample. The unidentified galaxies are mainly classified as ‘merged’ images in the APM galaxy survey, and thus not included in our catalogue. There is a very good correlation between the two estimates, but the scatter is rather large, with an *rms* of 0.35 mag. To investigate the cause of this dispersion, we have examined data from three fields (F157, F358 and F482) having more than 65 MDS galaxies in each, and have plotted them with different symbols in Figure 14. It is clear that the *rms* scatter for each plate is very small, only 0.16, 0.15 and 0.14 respectively. These scatters are slightly smaller than the typical *rms* uncertainties estimated from the APM plate overlaps. So, even if we assume that the MDS measurements are correct, and all of the scatter is due to the approximation involved in our simple method of estimating μ_0 , the errors introduced are smaller than the observational errors associated with measuring different UKST plates.

These three plates were deliberately chosen to lie at the extremes of the distribution plotted in Figure 13, and it is clear that the zero-points of these three plates are very different. The zero-point for field F358, is almost 1 mag away from other two plates. If our zero-point was in error by 1 mag, it would be clearly visible as a discrepant point in Figure 9. Also the area covered by field F358 would show up as a large overdensity in Figure 10(a), and an underdensity in Figure 10(c). None of these tests suggests there is any significant error in our zero-point for this plate, and so we believe the MDS zero-point is in error. Assuming that the *rms* error on our measurements is 0.16 mag as discussed in Section 4.3, this suggests that the MDS zero-points have an *rms* of 0.31 mag, and so F358 would be a 3 sigma deviation, which is not unexpected in a sample of around 100 plates.

MDS estimate that the uncertainty in their calibration is about 0.1 mag for plates with external calibration, and 0.2 for plates where they have used overlaps. There are two possible sources for the larger errors that we find. First, they do not apply any sort of vignetting or desensitization correction. Since their zero-points rely on edge matching and small-area CCD calibration data, this will introduce an error in the plate zero-points with an *rms* of order 0.1-0.2 mag. Second, MDS use the magnitudes of faint stars in the plate overlaps to estimate the zero-points on plates with no external calibration. Even faint stars tend to have a higher SB than galaxies, and this is likely to introduce a further bias. These two effects together might account for the observed 0.31 mag *rms* difference. This comparison shows that calibrating the zero-points of photographic data is a difficult problem that is still without a satisfactory solution.

Impey et al. (1996, hereafter ISIB) scanned 24 UKST survey plates to search for LSBGs with $\mu_0 > 22 \text{ mag arcsec}^{-2}$. Some of these plates are covered by the APM data used in this paper, and we find 202 galaxies in common with their data. Plots comparing the our magnitudes and surface brightnesses with the ISIB measurements are shown in Figure 15. There is a good correlation between the ISIB estimates and ours, but there are several differences in their analysis and definition of parameters which preclude a quantitative comparison with their data.

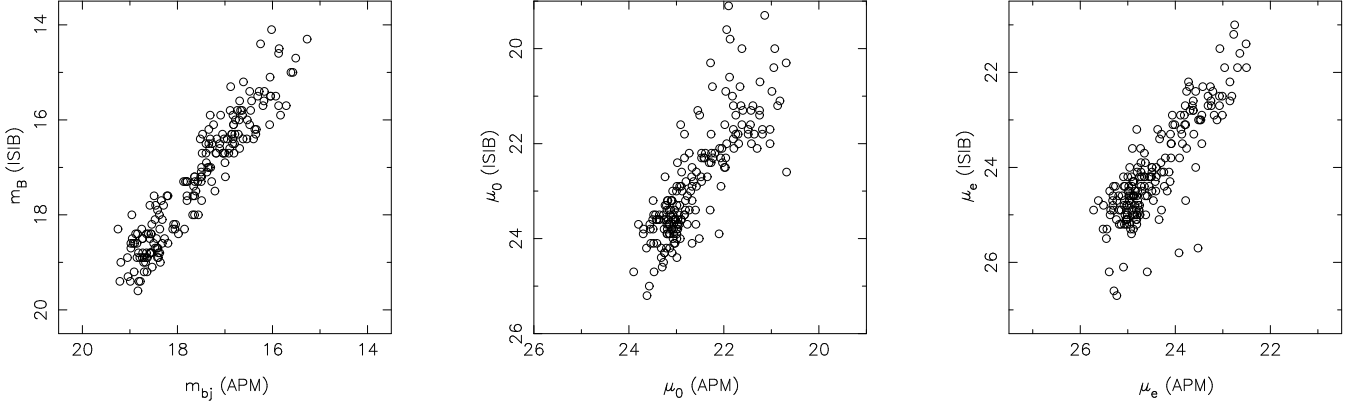


Figure 15. Comparison of total magnitude, central surface brightness and effective surface brightness of ISIB and this paper. Note that all data from ISIB are in the B band, while our APM results are in the b_J photographic band.

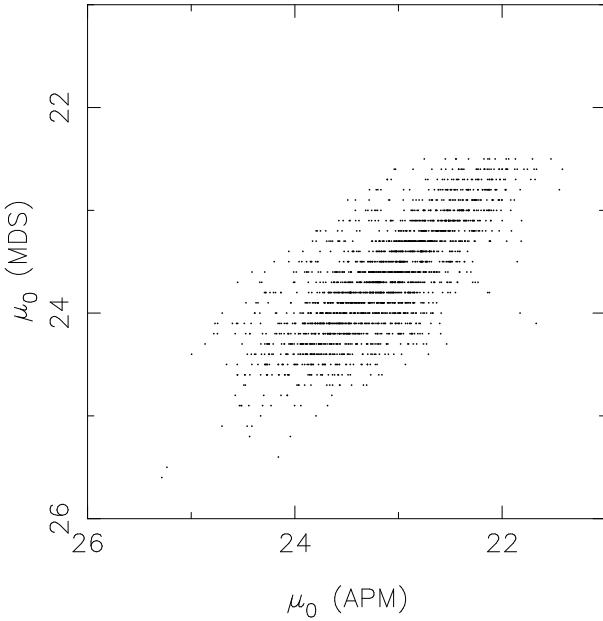


Figure 13. A comparison of central surface brightnesses of MDS and this paper. The dispersion is $\sigma = 0.35 \text{ mag arcsec}^{-2}$. To be consistent with MDS(1999), we have applied a correction to our μ_0 to account for the ellipticities of galaxies.

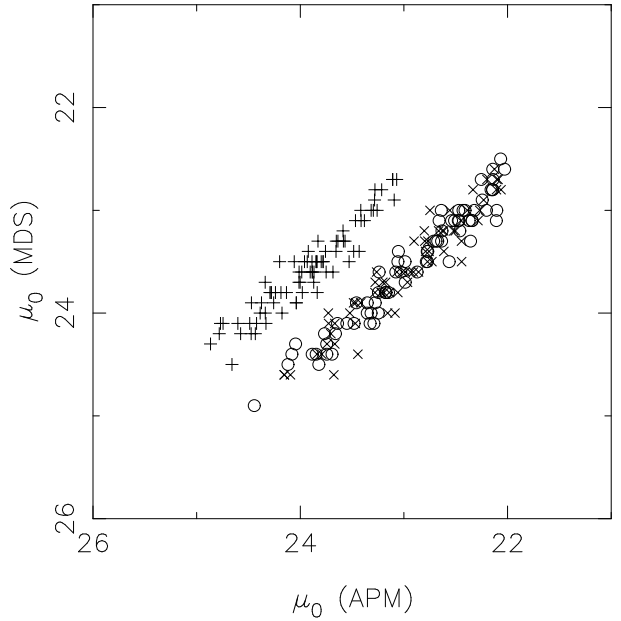


Figure 14. The same as figure 13 but showing data from only three independent plates which have more than 65 MDS galaxies on each. The three fields are: F157, which has an rms scatter of $0.16 \text{ mag arcsec}^{-2}$, is plotted with diagonal crosses; F358, which has an rms scatter of $0.15 \text{ mag arcsec}^{-2}$, is plotted with vertical/horizontal crosses; F482, which has an rms scatter of $\sigma = 0.14 \text{ mag arcsec}^{-2}$, is plotted with open circles.

5 DISCUSSION

5.1 The Distribution of Surface Brightnesses

Figure 16 shows a histogram of the frequency distribution of μ_0 . The distribution is centred on $\mu_0 = 22.2 \text{ mag arcsec}^{-2}$, and extends to $\mu_0 \simeq 20 \text{ mag arcsec}^{-2}$ at the high SB end, and to $\mu_0 \simeq 24.5 \text{ mag arcsec}^{-2}$ at the low SB end. The star-galaxy separation criteria (Maddox et al. 1990a) mean that some very high SB images will be rejected from the galaxy sample because their profile is so similar to stars. However, the rapid drop in the apparent number of high SB galaxies will be due to their small isophotal areas and a real drop in the space density of high SB galaxies (as shown by Cross et al. 2001). The lack of very low SB galaxies is less clearly a reflection of the true distribution of galaxy SBs, since a galaxy must have at least 4 square arcseconds brighter than

$25 \text{ mag arcsec}^{-2}$ to be selected in the APM galaxy sample. The distribution is further constrained by the 20.5 mag limit on the Gaussian profile magnitudes which will also bias against low SB galaxies. Cross et al. (2001) have used the 2dF Galaxy Redshift Survey to estimate the distribution of intrinsic surface brightnesses, and conclude that, although the APM selection criteria do exclude low SB galaxies, the missing galaxies would not contribute significantly to the overall luminosity density. We will consider how our selection criteria affect the observed distribution in a future paper.

It is clear from Figure 16 that the μ_0 subsamples plotted in Figure 10(a) and 10(c) represent the galaxies at the extremes of SB in the APM sample. This means that the

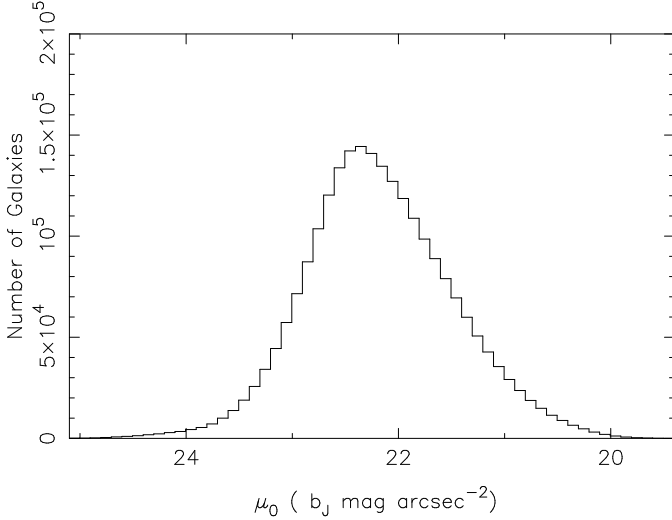


Figure 16. The frequency distribution of the apparent SB, μ_0 , for all galaxies in the survey.

distribution of galaxies in the sub-samples is very sensitive to any residual errors in the uniformity of the μ_0 measurements, and so the apparent uniformity of the galaxies in Figure 10(a) and 10(c) show that our corrections have given us a reliable and uniform set of μ_0 measurements.

5.2 The profiles of APM bright galaxies

In this Section, we use galaxies from the APM Bright Galaxy Catalogue (Loveday 1996; hereafter APMBGC) to investigate how the profile of a galaxy depends on its morphological type, and test if the assumption of an exponential profile is valid. The galaxies in the APMBGC have $b_J < 16.44$ and have a relatively large angular size (r_{iso}) and large σ^2 . Although σ^2 is not very sensitive to changes in the profile of galaxies, and the observational error is quite large, this parameter does contain useful information about the SB profile. Furthermore, the APMBGC galaxies have been morphologically classified by visual inspection of the UKS plates and we have analyzed the distribution of σ^2 separately for both early and late type galaxies.

We calculated the (p_0, r_0) of each galaxy, assuming an exponential SB profile as in Section 3. Since we also know the apparent ellipticity e for each galaxy (from the density weighted second moments), and the values of the detection threshold and saturation of the plate, we can simulate the observed APM density for each pixel. Any other observational parameters can then be estimated from this exponential model image. In particular, we have estimated the value of σ^2 , and compare this to the actual observed value. Obviously, if the original image is exactly an exponential profile, and there are no other observational errors, then the observed value, σ_{obs} will be exactly equal to that from the exponential model σ_{exp} , so the ratio $\sigma_{\text{obs}}/\sigma_{\text{exp}}$ should be exactly unity. To test the sensitivity of σ to variations in the SB profile, we created simulated images that follow the $r^{1/4}$ law profile (eq. 22), and analysed them using the assumption of an exponential profile. In this case we found that $\sigma_{\text{obs}}/\sigma_{\text{exp}} \simeq 0.9$, with a small variation according to their real central surface brightness and apparent elliptic-

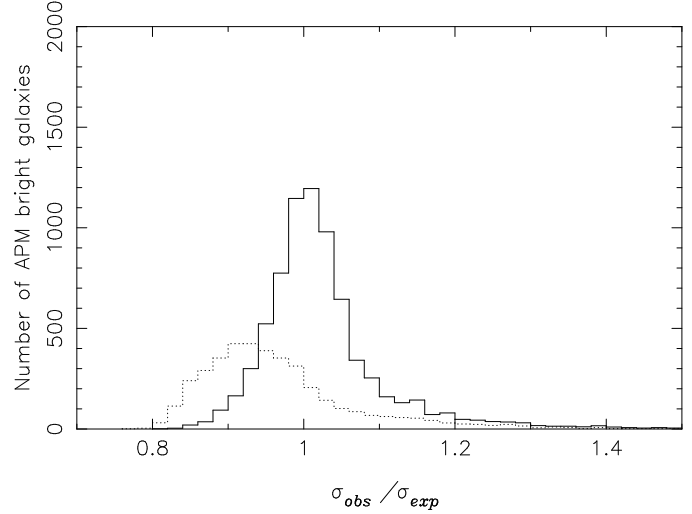


Figure 17. The frequency distribution of $\sigma_{\text{obs}}/\sigma_{\text{exp}}$ values for APM bright galaxies. The dotted line shows E and S0 galaxies; the solid line shows Spiral and Irr. An exponential profile would have $\sigma_{\text{obs}}/\sigma_{\text{exp}} = 1.0$, an $r^{1/4}$ law profile would have $\sigma_{\text{obs}}/\sigma_{\text{exp}} = 0.9$, and a Gaussian profile would have $\sigma_{\text{obs}}/\sigma_{\text{exp}} = 1.1$.

ity. The same analysis for Gaussian profiles gave a ratio of $\sigma_{\text{obs}}/\sigma_{\text{exp}} \simeq 1.1$.

In Figure 17, we plot the frequency distribution of $\sigma_{\text{obs}}/\sigma_{\text{exp}}$ for early and late galaxies from the APMBGC. There is a large dispersion in $\sigma_{\text{obs}}/\sigma_{\text{exp}}$, even for only late type galaxies. Nevertheless, the peak of the distribution is very close to 1.0, which implies that the exponential profile is a reasonable approximation for most galaxies (77% of the sample has $0.9 < \sigma_{\text{obs}}/\sigma_{\text{exp}} < 1.1$). For early type galaxies (E and S0), the dispersion is larger than for late type galaxies, and most of them have smaller $\sigma_{\text{obs}}/\sigma_{\text{exp}}$ values that are more consistent with an $r^{1/4}$ law profile. This shows that, although the APM measurements span a rather limited range of SB, the σ parameter can distinguish between early and late-type galaxies.

For fainter APM galaxies, the observational uncertainty on σ^2 will be much larger, and the small differences between the $r^{1/4}$, exponential and Gaussian assumptions mean that σ^2 is not effective in constraining the SB profile.

6 SUMMARY

We have described a simple method to estimate the central surface brightness, μ_0 , of galaxies, allowing for saturation and isophotal effects, and applied it to all the galaxies in the APM galaxy survey. We have corrected the μ_0 estimates for the effects of vignetting and differential desensitization over the field of each UKS plate. We have also used the plate overlap areas to match the individual plate measurements, and so provide homogeneous μ_0 estimates for all the APM galaxies. Internal and external checks of the uncertainties in μ_0 suggest that the uncertainty for an individual measurement is about 0.16 mag.

For very bright APM galaxies, the second radial moment of the SB profile, σ^2 , shows that late type galaxies are consistent with an exponential profile, whereas early type

galaxies have a higher mean SB, consistent with an $r^{1/4}$ law.

This uniform set of SB estimates for the APM galaxies will be used in later papers to select samples of high and low SB galaxies and analyze differences between their distributions.

ACKNOWLEDGEMENTS

Z.S. would like to thank all members of the astronomy group in Nottingham for their hospitality during his stay in Nottingham. Z.S. acknowledges support from grant NKBRSF G19990754 and the National Nature Sciences Foundation of China. This work was also partly supported by PPARC. We thank the referee for useful comments on the original manuscript. The comparison with CCD observations used the NASA Goddard Space Flight Center HDF-S public data recorded by J.P. Gardner and P. Palunas at the Cerro Tololo Inter-American Observatory, a division of the National Optical Astronomy Observatories. Further comparisons used the Anglo-Australian Observatory Hubble Deep Field-South public data, recorded by K. Glazebrook, R. Abraham and C. Tinney on the Anglo-Australian Telescope.

REFERENCES

- Bertin E., 1998, *SExtractor User's Guide*, Institut d'Astrophysique de Paris
- Bertin E., Arnouts S., 1996, A&AS, 117, 396
- Blair M., Gilmore G., 1982, PASP, 94, 742
- Cawson M. G. M., Kibblewhite E. J., Disney M. J., Philipps S., 1987, MNRAS, 224, 557
- Côté S., Broadhurst T., Loveday J., Kolind S., 1999, ASP Conference Series, 170, *The Low Surface Brightness Universe*. IAU Col. 171, 307
- Cross N., Driver S. P., Couch W. J., et al., 2001, MNRAS, 324, 825
- Dawe J. A., Metcalfe N., 1982, *Proc. astr. Soc. Aust.*, 4, 466
- de Jong R. S., 1996, A&AS, 118, 557
- de Jong R. S., van der Kruit P. C., 1994, A&AS, 106, 451
- Heraudeau P., Simien F., 1996, A&AS, 118, 111
- Impey C. D., Sprayberry D., Irwin M. J., Bothun, G. D., 1996, ApJS, 105, 209
- Jansen R. A., Franx M., Fabricant D., Caldwell N., 2000, ApJS, 126, 271
- Lambas D. G., Maddox S. J., Loveday J. 1992, MNRAS, 258, 404
- Lauberts A., Valentijn E. A., 1989, *The Surface Photometry Catalogue of the ESO-Uppsala Galaxies*. European Southern Observatory, Garching
- Loveday J., 1996, MNRAS, 287, 1025
- Maddox S. J., 1988. *PhD thesis*, University of Cambridge.
- Maddox S. J., Efstathiou G., Sutherland W. J., Loveday J., 1990a, MNRAS, 243, 692
- Maddox S. J., Efstathiou G., Sutherland W. J., 1996, MNRAS, 283, 1227
- Maddox S. J., Efstathiou G., Sutherland W. J., 1990b, MNRAS, 246, 433
- Morshidi-Esslinger Z. B., Davies J. I. & Smith R. M., 1999, MNRAS, 304, 297
- Palunas P., Collins N. R., Gardner J. P., Hill R. S., Malumuth E. M., Smette A., Teplitz H. I., Williger G. M., Woodgate B. E., 2000, ApJ, 541, 61
- Schlegel D., Finkbeiner D., Davis, M., 1998, ApJ, 500, 525
- Sprayberry D., Impey C., Irwin M., 1996, ApJ, 463, 535
- Teplitz H. I., Hill R. S., Malumuth E. M., Collins N. R., Gardner J. P., Palunas P., Woodgate B. E., 2001, ApJ, 548, 127
- Wittman D. M., Tyson J. A., Bernstein G. M., Lee R. W., dell'Antonio I. P., Fischer P., Smith D. R., Blouke M. M., 1998. Proc. SPIE Vol. 3355, 626